Article:
Zare Pakzad, Sina, Nasr Esfahani, Mohammad orcid.org/0000-0002-6973-2205 and Alaca, B. Erdem (2024) Mechanical properties of silicon nanowires with native oxide surface state. Materials Today Communications. 108321. ISSN 2352-4928

https://doi.org/10.1016/j.mtcomm.2024.108321

An Analytical-Atomistic Model for Elastic Behavior of Silicon Nanowires

May 2024

Abstract. Silicon nanowires entail significant potential as sensors in nanoelectromechanical systems. Despite its crucial impact in such applications, inconsistent trends in mechanical behavior reported in computational and experimental studies remain unexplained. Hence, scale effect in even the most fundamental elastic properties requires clarification. This work introduces a multiscale model to bridge the existing gap between atomistic simulations and experimental observations encountered around a critical dimension of 10 nm. The combined approach of this work is based on molecular dynamics and modified core-shell model and captures the scale effect over a substantial size range. The evolution of the modulus of elasticity is thus studied and linked to nanowire critical dimension through the parameterization of surface inhomogeneity. The developed method is also validated through an analysis of native oxide revealing an average modulus of elasticity of 75 GPa. The method's applicability can be extended to similar one-dimensional structures with unique surface states.

Keywords: Silicon nanowire, molecular dynamics, tensile behavior, native oxide, elastic modulus

Submitted to: *JPhys Materials*

1. Introduction

Silicon nanowires (Si NWs) exhibit a distinctive set of properties enabling their use in applications such as sensing, energy conversion and communication [1, 2, 3]. Compared to other one-dimensional nanostructures, the ease of their integration and miniaturization due to their compatibility with semiconductor manufacturing puts Si NWs in a unique position to serve as the main transducer building block in nanoelectromechanical systems (NEMS) and nanoelectronic devices [4, 5, 6, 7, 8]. There is extensive literature studying the effect of miniaturization on the physical properties of Si NWs as a prerequisite for the development of innovative applications [9, 10, 11, 12, 13, 14, 15, 16, 17, 18]. In this regard, Si NW mechanical properties have drawn considerable attention, where several discrepancies exist among reported trends regarding the dependence of mechanical behavior on scale [9, 11]. Furthermore, most nanomechanical tests on Si NWs were reported for a critical dimension (CD) in excess of 10 nm, while computational studies were mainly restricted to CDs below 10 nm. This

dimensional limitation from both experimental and computational perspectives has led to the loss of a common ground between the two approaches, thereby delaying the development of an understanding regarding the size dependence in Si NW mechanical properties [9, 10, 11].

Surface effects, the leading outcome of miniaturization, are found to be an important factor influencing NWs properties [9, 19]. The surface state pertains to the condition of a NW surface as identified by its physical, chemical, and structural properties. In the case of Si NWs, the surface state is commonly observed to be an amorphous silicon dioxide, or native oxide, layer covering Si core [13]. Native oxide is known to have significant effects such as reducing both the stiffness and strength [19, 20]. The formation of native oxide is also reported to cause a substantial intrinsic tensile stress up to 1.2 GPa in Si NWs [13]. Furthermore, a recent study highlighted the impact of the surface state and anisotropic surface properties on the mechanical properties of Si NWs. Hence, these parameters, identified as surface stress and surface elastic constants, need to be implemented into nanomechanical modeling [12, 14]. Moreover, implementation of surface effects into analytical modeling can be carried out through several analytical techniques.

In particular, core-surface [12, 21, 22], core-shell (CS) [23, 24] and modified core-shell (M-CS) [25, 26] models are extensively employed for this purpose. The CS model utilizes a core with the modulus of the bulk material and a shell that is coaxial with the core, where the surface modulus is correlated to the reduction in surface bond lengths [23, 24]. The CS model thus assumes an abrupt change of properties from core to the surface. Hence, the M-CS model was introduced to consider a gradual transition between core and surface properties [25, 26, 27]. So far, the surface state in the M-CS approach has been utilized for Si with unreconstructed surface state only, while the presence of a native oxide surface in Si NWs is widely reported in experimental observations [25, 26, 27].

This study proposes a new approach to incorporate molecular dynamics (MD) simulations into the M-CS model in order to bridge the 10-nm CD gap between experimental and computational approaches mentioned previously, thus providing a thorough understanding on the size-dependent elastic properties of Si NWs. The need for a multiscale modeling approach is clearly justified by recent compilation of data in review articles [9, 11]. In this approach, MD simulations will inform the surface properties, considering a native oxide layer, into the M-CS model to study NWs with CDs beyond 10 nm.

2. Methods

In this study, MD simulations are conducted using the modified Stillinger-Weber (m-SW) [28] and Tersoff-Munetoh (TM) [29] interatomic potentials. Compared to other potentials utilized for the modeling of Si and oxygen interactions, these two were found to be optimum for capturing the elastic properties of Si NWs with a native oxide surface

layer [12, 19, 30, 31]. Si NWs in different crystal orientations and with a diameter, (D), in the range of 4 nm to 8 nm (as an indication of CD) are considered. In the remainder of this work, the native oxide layer with its amorphous structure will be denoted as $aSiO_2$, and Si NWs with a native oxide layer (as opposed to those with an unreconstructed Si surface) are referred to as $aSiO_2$-Si NWs.

The flowchart presented in Fig. 1 outlines the computational methodology involving M-CS model combined with MD simulations. Both CS and M-CS models comprise a Si crystal core with a bulk modulus of elasticity, E_{Si}. In the CS model, the surface layer consists of native oxide ($aSiO_2$) with a constant modulus, E_{aSiO_2}. In the M-CS model, the modulus ($E_{aSiO_2}(r)$) is a function of r. Si core and native oxide surface are represented by grey and red colors, respectively, while the shaded grey layer in the M-CS model indicates the transition between bulk and surface. Atomic configurations in MD simulations are depicted over a circular cross-section of $aSiO_2$-Si NWs with a critical dimension, CD, of D and a native oxide thickness, t. Additionally, NW length (L), support region length (L_s), and movable region length (L_m) are indicated. Grey and red spheres represent Si and O atoms, respectively.

The M-CS model utilizes an exponential expression for the change of properties from bulk Si to the free surface of the native oxide layer for predicting the surface elasticity, where the surface modulus E_{aSiO_2} is expressed as a function of the surface radius, r, ranging from R_0 to R_0+t. Here, t denotes the native oxide thickness, while R_0 represents the radius of the Si core. In this model, Eqn.1 estimates the surface elasticity, with $E_{aSiO_2}(r)$ representing the change of the elastic property across the surface layer, which is a function of the Si core modulus of elasticity, denoted as E_{Si}. The surface factor parameter α establishes a relationship between the thickness, t, and a dimensionless constant $\tilde{\alpha}$, as $\alpha = \tilde{\alpha}/t$. The value of $\tilde{\alpha}$ determines the level of inhomogeneity in the elastic properties for the transition between the bulk crystal and the oxide surface. Additionally, the sign of $\tilde{\alpha}$ indicates whether the surface layer becomes stiffer (positive) or more compliant (negative) upon such transition.

$$E_{aSiO_2}(r) = E_{Si}e^{\alpha(r-R_0)} R_0 \leq r \leq R_0 + t \tag{1}$$

After estimating the modulus of elasticity for the native oxide layer (E_{aSiO_2}), the modulus of elasticity of the NW, E, can be calculated based on Eqn.2 [25, 26]. For further details on the M-CS model, interested reader is referred to the related literature [25, 26].

$$E = E_{Si}\Big[(1-\frac{2t}{D})^2 + \frac{4t}{\tilde{\alpha}D}(e^{\tilde{\alpha}} - (1-\frac{2t}{D})) - \frac{8t^2}{\tilde{\alpha}^2D^2}(e^{\tilde{\alpha}}-1)\Big] \tag{2}$$

MD simulations are performed on $aSiO_2$-Si NWs with the Si core along $< 100 >$, $< 110 >$, $< 111 >$, and $< 112 >$ crystal orientations using the LAMMPS code [32]. Circular NW cross-sections and an oblique view are depicted in Fig. 1. Non-periodic boundary conditions are applied in all directions. To ensure the compatibility between

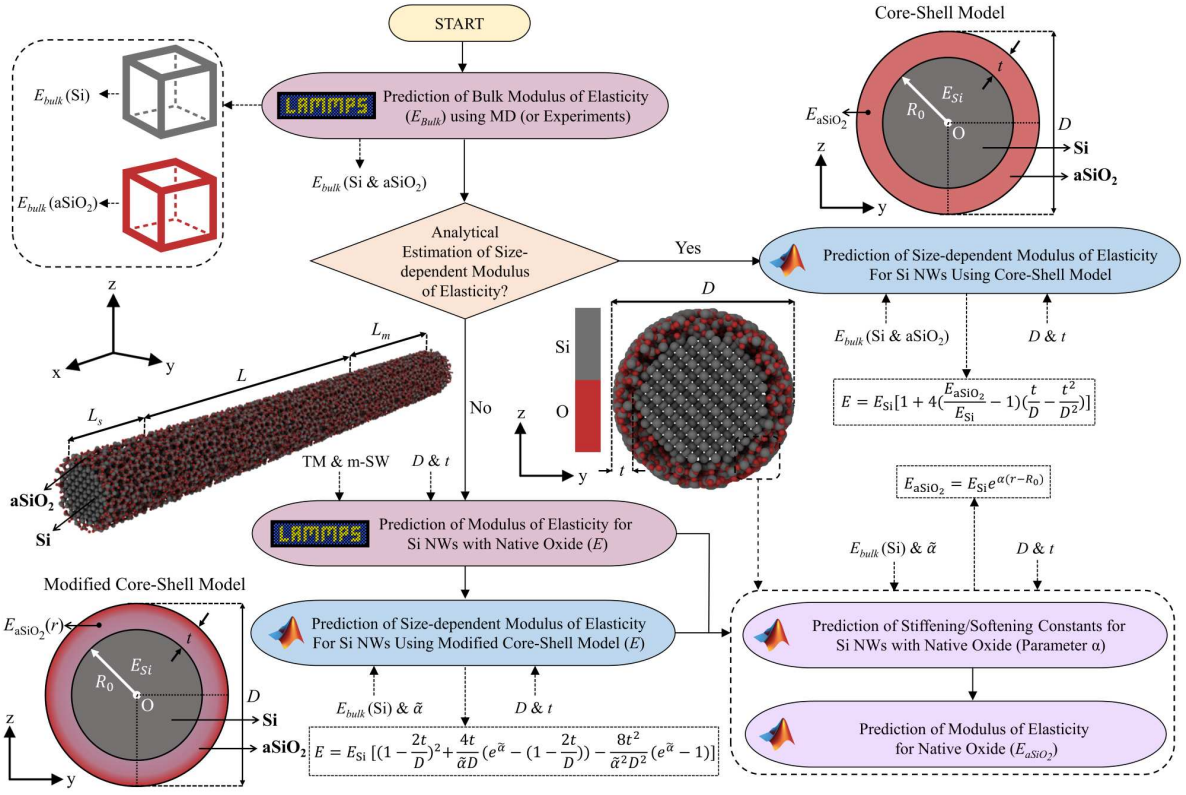

Figure 1. Flowchart depicting the methodology for the combination of Core-Shell (CS) and Modified Corse-Shell (M-CS) models with Molecular Dynamics (MD) to implement the native oxide surface state in the calculation of the Si NW elastic properties. Both models consist of a Si crystal core with a bulk modulus of elasticity, E_{Si}. For CS model, the surface layer is composed of native oxide, (aSiO$_2$), with a constant modulus, E_{aSiO_2}. For the M-CS model, the modulus, ($E_{aSiO_2}(r)$), is evolving as a function of r. Si core and native oxide surface are depicted by grey and red colors, respectively, with the shaded grey layer in M-CS model indicating the transition between bulk and surface. The atomic configuration in MD simulations is represented over a circular cross-section of aSiO$_2$-Si NWs with a critical dimension, CD, of D and a native oxide thickness, t. NW length (L), support region length (L_s), and movable region length (L_m) are also shown. The grey and red spheres represent Si and O atoms, respectively. The fitting process in the M-CS model involves assigning geometric inputs in alignment with MD results and incorporating specific assumptions about core Si elasticity. The adjustment of the surface elasticity parameter during fitting reveals the level of inhomogeneity for particular configurations within the M-CS model. Consequently, M-CS curves are generated for two oxide thicknesses and three distinct assumptions regarding core Si elasticity.

MD simulations and the M-CS method, this study examines Si NWs with circular cross-section only. A length-to-diameter (L/D) ratio of 10 is employed as a suitable limit for examining the elasticity of NWs through MD simulations [19, 20, 33]. It should be noted that the common cross-sections of Si NWs are typically circular (mostly $< 111 >$-Si and $< 112 >$-Si NWs through bottom-up synthesis) or rectangular (mostly $< 100 >$-Si and $< 110 >$-Si NWs through top-down manufacturing) [9, 19, 20]. The influence of NW cross-sectional shape on elastic properties can be found elsewhere [20].

Initially, atoms are assigned an initial velocity with a Gaussian distribution at a finite temperature of 300 K, followed by an energy minimization using the conjugate gradient method. Subsequently, all NWs are relaxed at 300 K for 50 ps using a time step of 1 fs in a canonical NVT ensemble. During the relaxation step, the support and movable regions of length L_s and L_m, respectively, are held in a fixed configuration with both lengths set equal to one-eighth of the total length, L. This allows one to capture the initial stresses induced by the surface at the beginning of the stress-strain curves [34]. In the next step, the tensile test is conducted by moving one end of the NW. To mitigate the shock wave resulting from high loading rates, a linearly varying constant velocity is applied along the longitudinal direction (x), ranging from zero at the support to the maximum velocity applied at the movable boundary. In this regard, a velocity of 1.0 $\mathring{A}$/ps at a temperature of 300 K is employed corresponding to a strain rate of $\dot{\epsilon} \approx 1.0 \times 10^9$ s^{-1}. Such a strain rate falls within the usual range utilized in MD-based NW tensile tests [19, 20, 30, 33]. Atomic stresses are determined by the virial theorem [35]. Bulk elastic properties of Si, E_{Si} ($E_{Exp.}$, E_{TM}, and E_{m-SW}), and native oxide, E_{aSiO_2}, are first modeled via the m-SW and TM potentials. Results listed in Table 1 and Table 2 in the Supplementary Information along with the corresponding experimental data [9] are found to align well with previous theoretical and MD findings [19, 36, 37]. Guided by these MD results, M-CS model is then employed to observe the size dependence of NW elasticity, E.

3. Results

Figs. 2 and 3 demonstrate the change of E as a function of D obtained from the combined MD and M-CS model for Si NWs fabricated via top-down ($< 100 >$ and $< 110 >$-oriented) and bottom-up ($< 111 >$ and $< 112 >$-oriented) methods, respectively. The fitting procedure within the M-CS model is executed by allocating geometrical inputs in a fashion consistent with MD results, while adopting distinct assumptions regarding core Si elasticity. The tuning of the surface elasticity parameter during the fitting process reveals the degree of inhomogeneity for specific configurations within the M-CS model. In this respect, the M-CS curves are obtained for two oxide thicknesses and three distinct core Si elasticity assumptions. Plots also include extensive data from previous experimental measurements [11]. Lines in both Figs. 2 and 3 represent the results of the combined analytical-atomistic approach of this work, conclusively negating the existence of a 10-nm barrier. Specifically, results show a significant size-dependent

E for $aSiO_2$-Si NWs for D less than 10 nm. In this regard, E changes up to 28% as D increases from 4 nm to 8 nm for a native oxide thickness, t, of 0.5 nm (solid lines) (Fig. 2). This change is very similar (about 32%) for bottom-up NWs (Fig. 3) for both m-SW and TM potentials. The size effect becomes more noticeable with an increase of t to 1.0 nm (dashed lines), where the same increase in D from 4 nm to 8 nm leads to a 29% to 51% change in E for $< 100 >$ and $< 110 >$, respectively (Fig. 2). Similarly, $< 111 >$-, and $< 112 >$-oriented NWs exhibit a stiffening in the range of 42% to 66% over a similar size range (Fig. 3). α predicted by M-CS model for both Figs. 2 and 3 is found to be within a very narrow range from -0.6 to -2.0, with the negative sign indicating the softening effect of the native oxide. Finally, TM potential is found to exhibit a higher degree of size-dependence compared to m-SW, although the trends are quite similar. Further details on the differences between the two potentials can be found elsewhere [19]. In particular, a similar understanding of elasticity concerning the relation between the native oxide and the crystal orientation of the core Si is evident in a prior investigation of the anisotropic surface properties of Si thin films with a native oxide layer [12]. This correlation can be associated with the influence of α in interpreting the interface between Si and the native oxide in Si NWs.

Model findings are also compared with extensive amount of experimental data, where the combined analytical-atomistic model of this work is constructed using E_{Si} derived from experimental measurements [9] in addition to MD simulations. For example, as no experimental report on $< 100 >$-oriented Si NWs with D below 100 nm is available, scale-dependence is provided only based on MD results (Fig. 2(a)). In contrast, thanks to the large amount of experimental data available on $< 110 >$-oriented Si NWs, a series of comparisons are provided in Fig. 2(b) [14, 38, 39, 40, 41, 42, 43, 44]. More specifically, when assigning experimental E_{Si}, the M-CS model aligns well with previous findings reported in experimental findings [38, 41, 42]. However, upon utilizing E_{Si} data from MD simulations, the M-CS model demonstrates a closer alignment with the reported E values from a separate series of experimental studies [14, 39, 40, 43, 44]. The primary lesson from Fig. 2(b) is the absence of any critical dimensional barrier between computational and experimental findings. That means effective atomistic modeling can indeed provide the necessary guidance to an analytical approach, facilitating the capture of scale dependence across a wide range of dimensions. Integrating MD outputs into the M-CS model establishes a link between the analytical approach and the interface of Si and native oxide. In the absence of MD outputs, the M-CS model primarily relies on estimation through fitting, resembling the CS model. However, by utilizing MD simulations, there is more capacity to understand the elastic properties of Si NWs with CDs of 10-nm, where employing full atomic simulations is computationally challenging.

The same methodology is then applied to $< 111 >$ and $< 112 >$ orientations as depicted in Fig. 3. $< 111 >$ is another crystalline orientation for which a wealth of modulus data is available in experimental studies. The MD calculations of elasticity for $< 111 >$-oriented $aSiO_2$-Si NWs with follow-up M-CS predictions of different oxide layer thickness assumptions linking the atomistic predictions to experimental

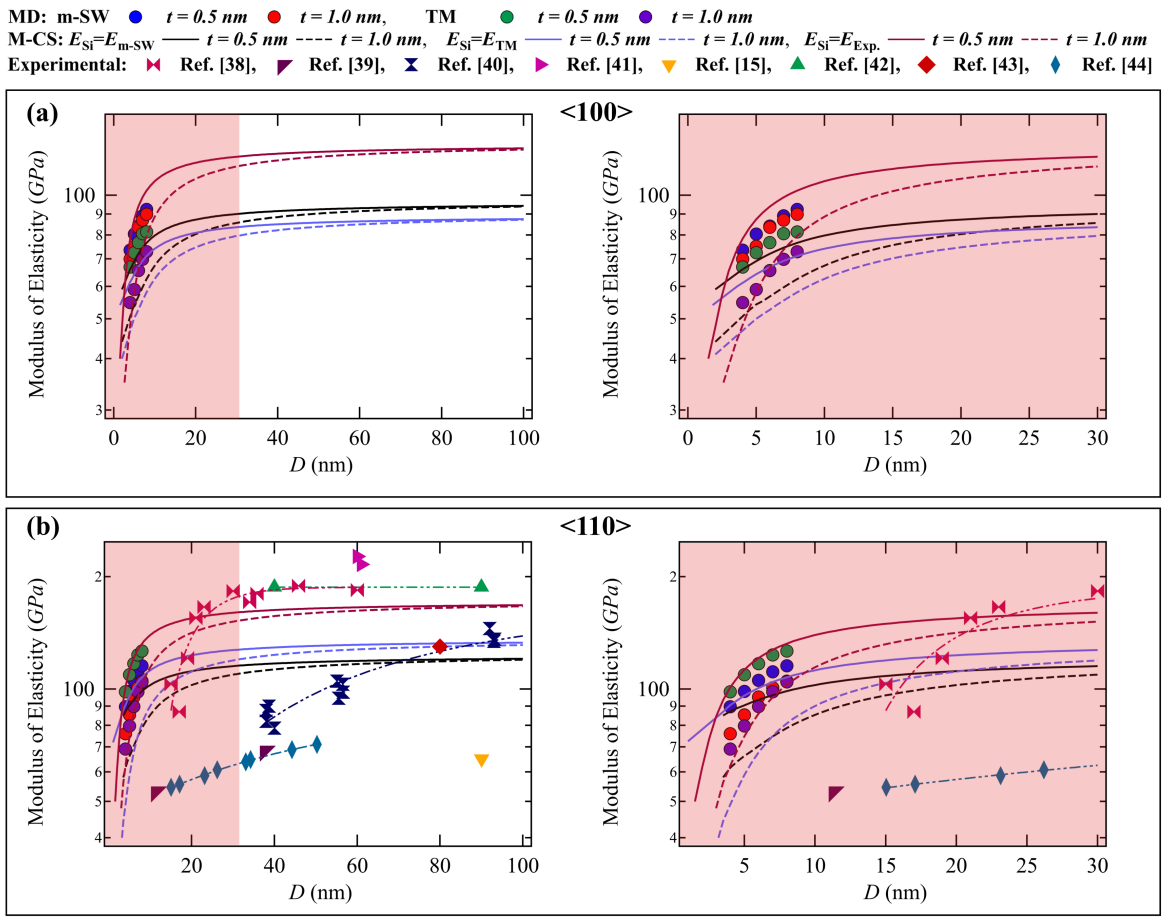

Figure 2. The modulus of elasticity, E, for $aSiO_2$-Si NWs in (a) $< 100 >$ and (b) $< 110 >$ crystal orientations. MD simulations are used to predict the E_{Si} along with experimental values while combined with M-CS model of this work. Experimental data [38, 39, 40, 41, 14, 42, 43, 44] is plotted by extracting the modulus of elasticity (E) from each respective study and utilizing it in the analysis of E as a function of D.

findings are elaborated further. Given M-CS estimations for $< 111 >$-oriented Si NWs considering the observed deviations due to multiple E_{Si} and t assumptions align well with experimental predictions [38, 45, 46, 47, 48, 49] given in Fig. 3(a). The M-CS model extends within both 100 nm and 30 nm ranges, as separately depicted in Fig. 3(b). Moreover, consistent with the findings of Zhu *et al.* [38], the combined M-CS and atomistic methods reveal an increasing trend in E for $< 111 >$-oriented Si NWs, further validating the accuracy of the M-CS model in capturing the size effect where experimental and computational trends are in proper agreement within the developed analytical-atomistic framework of this work. Given significant disparities between predicted experimental E for Si NWs, it is crucial to identify outliers within the established methodology, with Refs. [48, 49] highlighting some of these outliers. For $< 112 >$-oriented Si NWs of Fig. 3(b), M-CS model exhibits a good agreement with MD predictions as D increases. Despite the limited availability of experimental data for $< 112 >$-oriented Si NWs [50], the M-CS model, built upon experimental E_{Si},

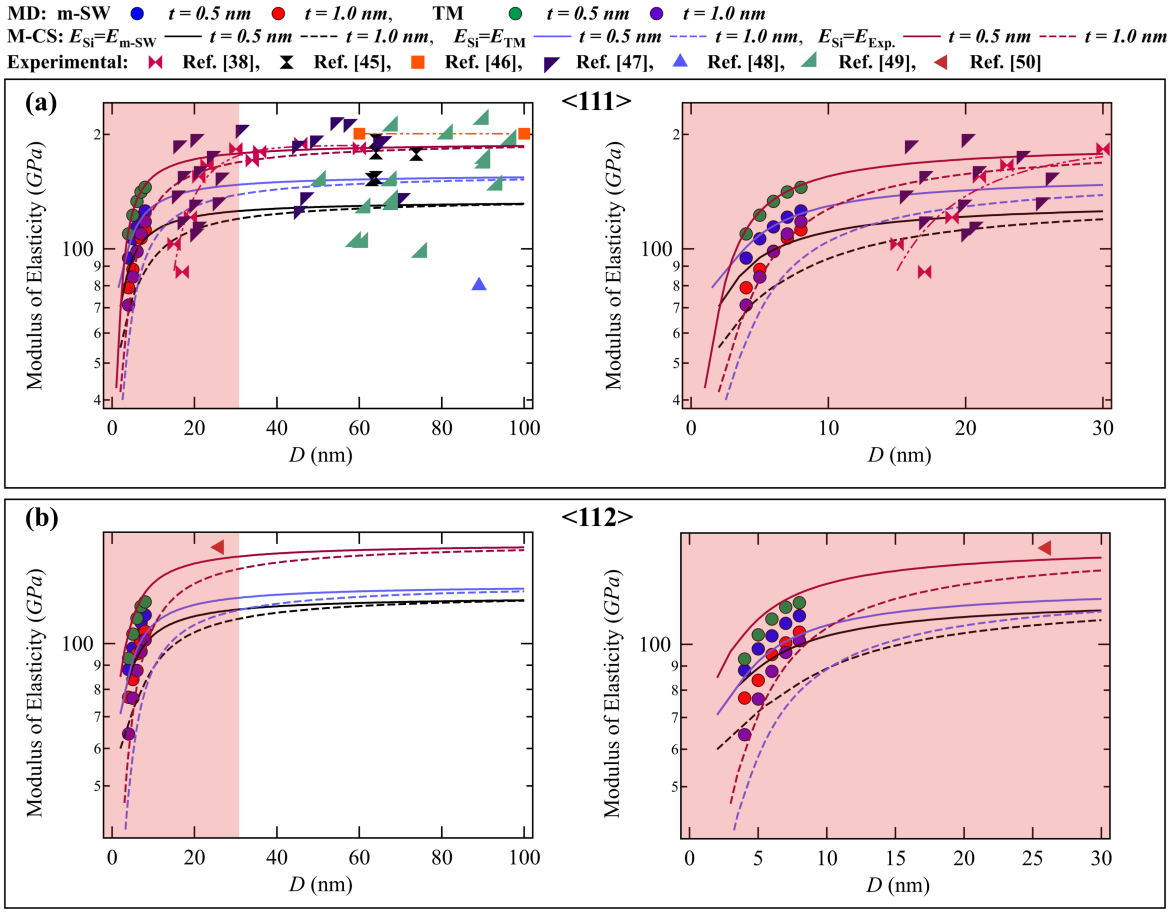

Figure 3. The modulus of elasticity, E, for $aSiO_2$-Si NWs in (a) $< 111 >$ and (b) $< 112 >$ crystal orientations. MD simulations are used to predict the E_{Si} along with experimental values while combined with M-CS model of this work. Experimental data [38, 45, 46, 47, 48, 49, 50] is plotted by extracting the modulus of elasticity (E) from each respective study and utilizing it in the analysis of E as a function of D.

offers a reliable trend, effectively addressing the transition from MD calculations to the experimental observations.

It should be emphasized that the limited available experimental data for $< 100 >$ and $< 112 >$ Si NWs leads to challenges in drawing definitive conclusions based on the findings depicted in Fig. 2(a) and Fig. 3(b). However, the observed size-dependent behavior of E for $< 110 >$ and $< 111 >$ Si NWs in Fig. 2(b) and Fig. 3(a) highlights the reliability of the proposed methodology to bridge the 10-nm barrier between computational and experimental findings and unite them forming a global trend. Unlike previous MD investigations on Si NWs with unreconstructed surfaces, which struggled to address computational and experimental reports on the size effect [11, 9], the present study successfully demonstrates the size-dependence in the modulus of elasticity of Si NWs. By incorporating the native oxide surface state, a direct connection is now established between the MD estimations and analytical methods. An examination on the performance of the CS and M-CS models is presented in the Supplementary Information

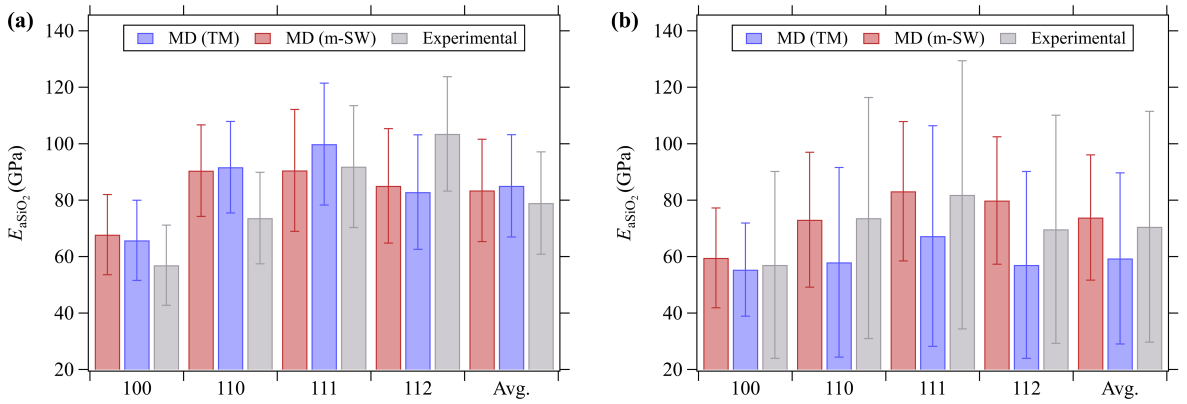

Figure 4. Modulus of elasticity of the native oxide (E_{aSiO_2}) estimated using the M-CS model under two oxide thickness assumptions: (a) $t = 0.5$ nm and (b) $t = 1.0$ nm. Estimations are based on three approaches: MD predictions using the TM and m-SW potentials, as well as experimental calculations. Results are presented for four crystal orientations of core-Si, namely $< 100 >$, $< 110 >$, $< 111 >$, and $< 112 >$, with the average value shown separately.

and it becomes clear that there is an inconsistency between the CS and M-CS models to predict the size effect on the elastic properties of Si NWs. For example, the scale dependence prediction by the CS model in Supplementary Information Fig.1 (a) exhibits the opposite trend as predicted by MD. This can be linked to the bulk modulus used in the CS model to predict E for $aSiO_2$-Si NWs with D below 8 nm. Furthermore, the CS model treats the core and sell elastic properties independent, which overlooks interface effects between the core Si and native oxide, resulting in reduced accuracy as studied elsewhere [19]. In contrast, the M-CS model, once integrated with MD outputs, produces reliable outcomes across various critical dimension ranges particularly examined for four distinct crystal orientations of Si. This results in the development of an analytical atomistic approach, enabling a better understanding of the size effect on the elastic properties of Si NWs.

Due to the importance of insight obtained here regarding the role of the native oxide in understanding the size effect in Si NW elastic behavior, the elasticity of the native oxide is studied in greater detail. Utilizing the M-CS formulation outlined in Eqn. 2, the estimation of E_{aSiO_2} is performed for various combinations of Si core crystalline orientation and t using Eqn. 1. This is achieved by linking the dimensionless constant calculation conducted earlier and utilizing Eqn. 1 to derive the elasticity for the native oxide layer. The corresponding results are presented in Fig. 4(a) and Fig. 4(b) for the case of $t = 0.5$ nm and $t = 1.0$ nm, respectively. Data are tabulated in Table 3 of the Supplementary Information. Analysis of the findings reveals an average E_{aSiO_2} of 75 ± 28.6 GPa, a finding in very good agreement with previous experimental reports on bulk $aSiO_2$ [51]. Tabulated data elucidating the predictive capabilities of the M-CS model regarding bulk $aSiO_2$ modulus of elasticity are provided in the Supplementary Information. It is important to note that the limitations associated with the CS models

in accurately capturing the actual changes in elasticity from the core to the shell region have been previously reported [19]. Thus, it is observed that the M-CS model guided by proper MD estimations can generate more robust trendlines. This method not only reveals the size effect but also calculates the native oxide modulus at the nanoscale, marking the first instance of such calculation in the literature, to the best of our knowledge. The examination related to the CS model is also carried out with detailed explanations and accompanying graphs provided in the Supplementary Information.

4. Conclusion

Comparison with vast data obtained on Si NWs during two decades of nanomechanical testing is one of the best validation techniques. For this purpose, this study focused on utilizing analytical modeling enabled by atomistic simulations to address the size effect studied in previous experimental literature. While no experimental data exists for $<100>$-oriented Si NWs with D below 100 nm, scale-dependence is examined via MD-based findings. Conversely, for $<110>$-oriented Si NWs, numerous comparisons are made with experimental data. In case of using experimental E_{Si}, *i.e.*, $E_{Exp.}$, the M-CS model aligns well with the previous experimental findings. The extended methodology to $<111>$-oriented Si NWs by having experimental data provides a robust model aligned with experimental findings, demonstrating the effectiveness of M-CS model to predict the size effect. Similarly, for $<112>$-oriented Si NWs, despite limited experimental data, the M-CS model provides reliable trends, bridging the gap between MD calculations and experimental observations. In conclusion, this study comprehensively examines the size effect in Si NWs through the integration of atomistic and analytical methods. By establishing a connection between experimental observations and atomistic predictions for Si NWs in various orientations, this study successfully resolves the longstanding challenge of reconciling these two approaches, particularly across the 10-nm CD barrier.

Data Availability Statement

The data that support the findings of this study are available from the corresponding author upon reasonable request.

Conflict of Interest

The authors have no conflicts to disclose.

References

[1] Badawy G and Bakkers E P 2024 *Chemical Reviews* **124** 2419–2440
[2] Nehra M, Dilbaghi N, Marrazza G, Kaushik A, Abolhassani R, Mishra Y K, Kim K H and Kumar S 2020 *Nano Energy* **76** 104991

[3] Yang L, Huh D, Ning R, Rapp V, Zeng Y, Liu Y, Ju S, Tao Y, Jiang Y, Beak J, Leem J, Kaur S, Lee H, Zheng X and S Prasher R 2021 *Nature communications* **12** 3926

[4] Zafar S, D'Emic C, Jagtiani A, Kratschmer E, Miao X, Zhu Y, Mo R, Sosa N, Hamann H, Shahidi G and Riel H 2018 *Acs Nano* **12** 6577–6587

[5] Sage E, Sansa M, Fostner S, Defoort M, Gély M, Naik A K, Morel R, Duraffourg L, Roukes M L, Alava T, Jourdan G, Colinet E, Masselon C, Brenac A and Hentz S 2018 *Nature communications* **9** 1–8

[6] Tintelott M, Pachauri V, Ingebrandt S and Vu X T 2021 *Sensors* **21** 5153

[7] Sreejith S, Ajayan J, Uma Reddy N and Manikandan M 2023 *Silicon* 1–27

[8] Tran V A, Vo G N, Vo T T T, Doan V D, Vo V and Le V T 2023 *Processes* **11** 1739

[9] Nasr Esfahani M and Alaca B E 2019 *Advanced Engineering Materials* **21** 1900192

[10] Wang S, Shan Z and Huang H 2017 *Advanced Science* **4** 1600332

[11] Yang C, Van Der Drift E and French P 2022 *Journal of Micromechanics and Microengineering* **32** 103002

[12] Zare Pakzad S, Nasr Esfahani M, Tasdemir Z, Wollschläger N, Li T, Li X, Yilmaz M, Leblebici Y and Alaca B E 2023 *ACS Applied Nano Materials* **6** 15465–15478

[13] Nasr Esfahani M, Zare Pakzad S, Li T, Li X, Tasdemir Z, Wollschlager N, Leblebici Y and Alaca B E 2022 *ACS Applied Nano Materials*

[14] Zare Pakzad S, Nasr Esfahani M, Tasdemir Z, Wollschlaeger N, Li X, Li T, Yilmaz M, Leblebici Y and Alaca B E 2021 *Mrs Advances* **6** 500–505

[15] Namazu T 2023 *IEEJ Transactions on Electrical and Electronic Engineering* **18** 308–324

[16] Zare Pakzad S, Ali B, Coban S B, Karimzadehkhouei M and Alaca B E 2023 Innovative mems stage for automated micromechanical testing *2023 International Conference on Manipulation, Automation and Robotics at Small Scales (MARSS)* (IEEE) pp 1–6

[17] Zare Pakzad S, Akinci S, Karimzadehkhouei M and Alaca B E 2023 *Semiconductor Science and Technology* **38** 125005

[18] Zare Pakzad S, Nasr Esfahani M, Canadinc D and Alaca B E 2024 *arXiv preprint at SSRN 4791813*

[19] Zare Pakzad S, Nasr Esfahani M and Alaca B E 2023 *Materials Today Communications* **34** 105002

[20] Zare Pakzad S, Nasr Esfahani M and Alaca B E 2024 *Materials Today Communications* **38** 108321 ISSN 2352-4928

[21] Gurtin M E and Ian Murdoch A 1975 *Archive for rational mechanics and analysis* **57** 291–323

[22] Stan G, Krylyuk S, Davydov A, Vaudin M, Bendersky L A and Cook R F 2008 *Applied Physics Letters* **92** 241908

[23] Miller R E and Shenoy V B 2000 *Nanotechnology* **11** 139

[24] Chen C Q, Shi Y, Zhang Y S, Zhu J and Yan Y J 2006 *Physical review letters* **96** 075505

[25] Yao H, Yun G, Bai N and Li J 2012 *Journal of Applied Physics* **111** 083506

[26] Xu X J, Wang Y C, Wang B and Zhang K 2016 *Physica E: Low-dimensional Systems and Nanostructures* **80** 53–61

[27] Li J, Lei X, Ding J, Gao Z, Wang H and Shi Y 2022 *Materials Letters* **307** 131001

[28] Ganster P, Treglia G and Saul A 2010 *Physical Review B* **81** 045315

[29] Munetoh S, Motooka T, Moriguchi K and Shintani A 2007 *Computational Materials Science* **39** 334–339

[30] Pakzad S Z, Esfahani M N and Alaca B E 2021 Molecular dynamics study of orientation-dependent tensile properties of si nanowires with native oxide: Surface stress and surface energy effects *2021 IEEE 21st International Conference on Nanotechnology (NANO)* (IEEE) pp 370–373

[31] Zare Pakzad S, Nasr Esfahani M and Alaca B E 2023 *arXiv preprint arXiv:2308.13610*

[32] Plimpton S 1995 *Journal of computational physics* **117** 1–19

[33] Kang K and Cai W 2007 *Philosophical Magazine* **87** 2169–2189 ISSN 14786435

[34] Li S and Gao X L 2013 *Handbook of micromechanics and nanomechanics* (CRC Press)

[35] Cormier J, Rickman J M and Delph T J 2001 *Journal of Applied Physics* **89** 4198 ISSN 00218979

[36] Ilinov A and Kuronen A 2014 *Journal of Applied Physics* **115** 104305

[37] Park S H, Kim J S, Park J H, Lee J S, Choi Y K and Kwon O M 2005 *Thin Solid Films* **492** 285–289 ISSN 00406090
[38] Zhu Y, Xu F, Qin Q, Fung W Y and Lu W 2009 *Nano letters* **9** 3934–3939
[39] Li X, Ono T, Wang Y and Esashi M 2003 *Applied Physics Letters* **83** 3081–3083
[40] Sadeghian H, Yang C, Goosen J, Van Der Drift E, Bossche A, French P and Van Keulen F 2009 *Applied Physics Letters* **94** 221903
[41] Tsuchiya T, Hemmi T, Suzuki J y, Hirai Y and Tabata O 2018 *Applied Sciences* **8** 880
[42] Hsin C L, Mai W, Gu Y, Gao Y, Huang C T, Liu Y, Chen L J and Wang Z L 2008 *Advanced Materials* **20** 3919–3923
[43] Zhang H, Tersoff J, Xu S, Chen H, Zhang Q, Zhang K, Yang Y, Lee C S, Tu K N, Li J and Lu Y 2016 *Science advances* **2** e1501382
[44] Han X, Zheng K, Zhang Y, Zhang X, Zhang Z and Wang Z L 2007 *Advanced Materials* **19** 2112–2118
[45] Gordon M J, Baron T, Dhalluin F, Gentile P and Ferret P 2009 *Nano letters* **9** 525–529
[46] San Paulo A, Bokor J, Howe R, He R, Yang P, Gao D, Carraro C and Maboudian R 2005 *Applied Physics Letters* **87** 053111
[47] Kim Y J, Son K, Choi I C, Choi I S, Park W I and Jang J i 2011 *Advanced Functional Materials* **21** 279–286
[48] Sohn Y S, Park J, Yoon G, Song J, Jee S W, Lee J H, Na S, Kwon T and Eom K 2010 *Nanoscale research letters* **5** 211–216
[49] Heidelberg A, Ngo L T, Wu B, Phillips M A, Sharma S, Kamins T I, Sader J E and Boland J J 2006 *Nano letters* **6** 1101–1106
[50] Stan G, Krylyuk S, Davydov A, Levin I and Cook R F 2012 *Nano letters* **12** 2599–2604
[51] Silva E C, Tong L, Yip S and Van Vliet K J 2006 *Small* **2** 239–243